ADVANCED ENERGY MATERIALS
www.advenergymat.de

Materials Views
www.MaterialsViews.com

Optical Absorption Enhancement in Freestanding GaAs Thin Film Nanopyramid Arrays

Dong Liang, Yijie Huo, Yangsen Kang, Ken Xingze Wang, Anjia Gu, Meiyueh Tan, Zongfu Yu, Shuang Li, Jieyang Jia, Xinyu Bao, Shuang Wang, Yan Yao, H.-S. Philip Wong, Shanhui Fan, Yi Cui,* and James S. Harris**

Although III–V compound semiconductor multi-junction cells show the highest efficiency among all types of solar cells, their cost is quite high due to expensive substrates, long epitaxial growth and complex balance of system components. To reduce the cost, ultra-thin films with advanced light management are desired. Here effective light trapping in freestanding thin film nanopyramid arrays is demonstrated and multiple-times light path enhancement is realized, where only 160 nm thick GaAs with nanopyramid structures is equivalent to a 1 μm thick planar film. The GaAs nanopyramids are fabricated using a combination of nanosphere lithography, nanopyramid metal organic chemical vapor deposition (MOCVD) growth, and gas-phase substrate removal processes. Excellent optical absorption is demonstrated over a broad range of wavelengths, at various incident angles and at large-curvature bending. Compared to an equally thick planar control film, the overall number of photons absorbed is increased by about 100% at various incident angles due to significant antireflection and light trapping effects. By implementing these nanopyramid structures, III–V material usage and deposition time can be significantly reduced to produce high-efficiency, low-cost thin film III–V solar cells.

1. Introduction

III–V material has been widely used in optoelectronic devices such as solar cells, light emitting diodes, lasers and detectors, due to the advantages of their direct bandgap, wide spectral coverage with matched lattice, and excellent absorbing and emitting properties. State-of-art III–V compound semiconductor multijunction cells have demonstrated the highest efficiencies among all types of solar cells.[1,2] A record high efficiency of 43.5% was achieved recently by Solar Junction.[2] The application of these cells, however, are limited to high concentration systems because of their high cost. If their cost can be reduced, large area application of high efficiency III–V solar panels might be possible and could have a significant impact on solar technologies. The high cost of III–V compound semiconductor solar cell is mainly from two aspects: one is from substrates such as GaAs or Ge. These wafers are usually over 10 times more expensive than Si wafers. To reduce the cost, III–V thin film epitaxial lift-off technology has been developed to release the solar cell device from the substrate, which can then be reused for successive growths.[3–5] Such a thin film also increases the cell efficiency due to enhanced optical confinement[5] and higher carrier density.[6] With the epitaxial lift off technique, a single junction GaAs solar cell achieved a record efficiency of 28.1%.[2,6] The second main cost of III–V cells is from the epitaxial deposition using metal organic chemical vapor deposition (MOCVD) or molecular beam epitaxy (MBE). A typical III–V solar cell requires a thickness of several micrometers to absorb all of the incoming photons. The growth time for such a cell can be several hours. To save the epitaxial growth material and to increase the throughput of the MOCVD or MBE growth, it is desirable to reduce the thickness of these solar cell layers, which requires light absorption enhancement techniques. Adding back-reflecting metal reduces the epitaxial layer thickness by about 30% while retaining the photocurrent and the overall efficiency of a single junction GaAs thin film cell.[5] However, reducing the epitaxial thickness to 1 μm or less would result in a significant loss of absorption. Therefore, new light trapping engineering strategies are needed to improve the absorption in order to further reduce the epitaxial growth thickness to a few hundred nanometers.

Nanostructures, such as nanowires,[7–10] nanorods[11] and nanocones[12,13] have been proposed to enhance light

D. Liang, S. Li
Department of Physics
Stanford University
Stanford, CA, 94305, USA
E-mail: dongl@stanford.edu
Y. Huo, Y. Kang, M. Tan, Z. Yu, J. Jia, X. Bao, S. Wang, Prof. H.-S. P. Wong, Prof. S. Fan, Prof. J. S. Harris
Department of Electrical Engineering
Stanford University
Stanford, CA, 94305, USA
E-mail: harris@snow.stanford.edu
K. X. Wang, A. Gu
Department of Applied Physics
Stanford University
Stanford, CA, 94305, USA
Y. Yao, Prof. Y. Cui
Department of Materials Science and Engineering
Stanford University
Stanford, CA, 94305, USA
E-mail: yicui@stanford.edu

DOI: 10.1002/aenm.201200022

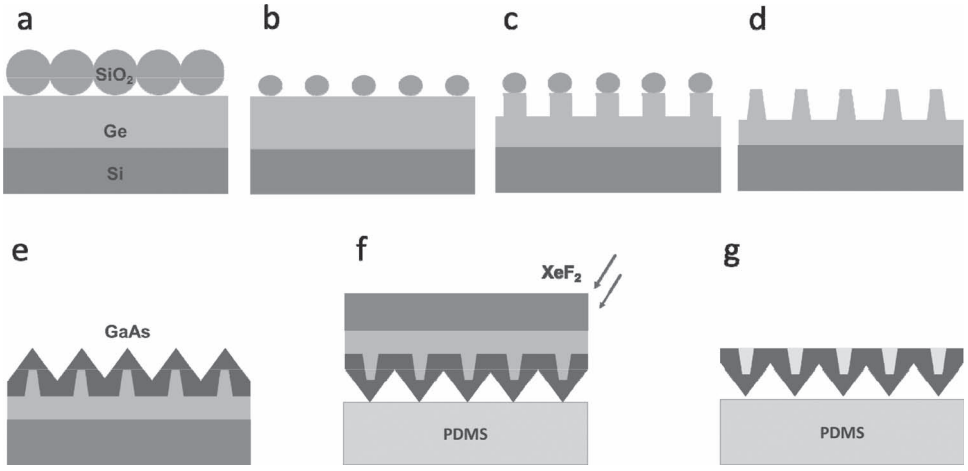

Figure 1. Schematic illustration of GaAs nanopyramid thin film fabrication. a) Silica nanospheres assembled into a close-packed monolayer on an epi-Ge substrate. b) Shrunk nanospheres. c) Ge nanopillars. d) Ge nanopyramids. e) GaAs-Ge core-shell nanopyramids. f) A flipped sample of GaAs-Ge core-shell nanopyramids attached to PDMS superstrate exposed to XeF_2 gas etching environment. g) A GaAs nanopyramid thin film on PDMS superstrate after substrate removal.

absorption and improve solar cell efficiencies in c-Si, CdTe, a-Si, etc. These nanostructures provide antireflection coating and absorption enhancement effects. Their three-dimensional design decouples light absorption and carrier separation, thus increasing internal quantum efficiency.[14] Although generally the taper shape is more effective in absorption than straight pillars due to the more gradual change of average refractive index, optimal nanostructures may vary in different photovoltaic materials. Material properties, such as crystal structures, absorption coefficients and minority carrier diffusion lengths need to be considered in optimizing nanostructures for both light management and overall solar cell performance.

For III–V compound semiconductors, crystalline quality can significantly affect the minority carrier life time. Therefore, maintaining good crystalline quality during nanoscale light trapping engineering is important. A recent study on GaAs cell uses vertical core-shell nanopillars to deomonstrate the concept of nanostructures in III–V phtovoltaics.[15] However, these nanopillars are on bulk substrate, not tapered and require e-beam lithography to fabricate.

In this paper, we introduce nanopyramids[16] in III–V thin films. Compared to previously reported nanostructures in III–V solar cells,[15,17] the nanopyramid thin film not only provides an adiabatic change of the effective refractive index at the front side, but also provides additional trapping from the confinement of backside nanostructures. Therefore, optical absorption in GaAs thin films can be significantly improved by implementing nanopyramids. In addition, nanopyramids preserve clear crystalline facets that indicate low defect density thus low non-radiative recombination rate desired in high efficiency single crystal III–V solar cells. Such nanopyramids could potentially reduce the thickness of the epitaxial absorbing layers in III–V solar cells by an order of magnitude to only a few hundred nanometers thus reduce the total cost.

2. Results and Discussion

2.1. GaAs Nanopyramid Thin Film Fabrication and Characterization

To prepare nanopyramid epitaxial germanium templates for GaAs growth, a 2 μm Ge buffer layer was first epitaxially grown on a 10 mm Si (100) wafer by chemical vapor deposition. This strain relaxed Ge epitaxial layer is lattice-matched to GaAs and shows a modest defect density of around 1×10^8 cm^{-2}.[18] We then apply silica nanosphere lithography, which is schematically illustrated in **Figure 1**a–d with corresponding scanning electron microscope (SEM) images of each step in **Figure 2**a–d, to fabricate Ge nanopyramid template. First, a monolayer of silica nanospheres was uniformly assembled on top of the epi-Ge substrate by spin coating (Figure 1a and 2a). These silica nanospheres were then decreased in size by oxide reactive ion etching (Figure 1b and 2b). Using these smaller silica nanospheres as an etching mask, Ge epitaxial layer was selectively etched down forming nanopillars of 500 nm in height and 200 nm in diameter (Figure 1c and 2c). After removing the silica nanosphere residue with dilute hydrofluoric acid and 30 sec wet etching in a nitric acid and hydroperoxide water solution, Ge nanopyramids (Figure 1d and 2d) were formed.

A thin GaAs layer (Figure 1e) was then grown on the these nanopyramid templates by metal organic chemical vapour deposition (MOCVD).[19] The nanopyramid growth condition was optimized to maintain uniform initial nucleation of GaAs on top of the 3D nanostructured Ge while providing sufficient surface mobility to maintain good crystal quality. After the MOCVD growth, GaAs/Ge core-shell nano-pyramids were observed and characterized with SEM (Figures 2e,f, **Figures 3**a,c,d). Figure 2e shows a 45° SEM image of these nano-pyramids with clear facets indicating excellent crystalline quality. A cross-section view of a single GaAs-Ge core-shell pyramid is demonstrated

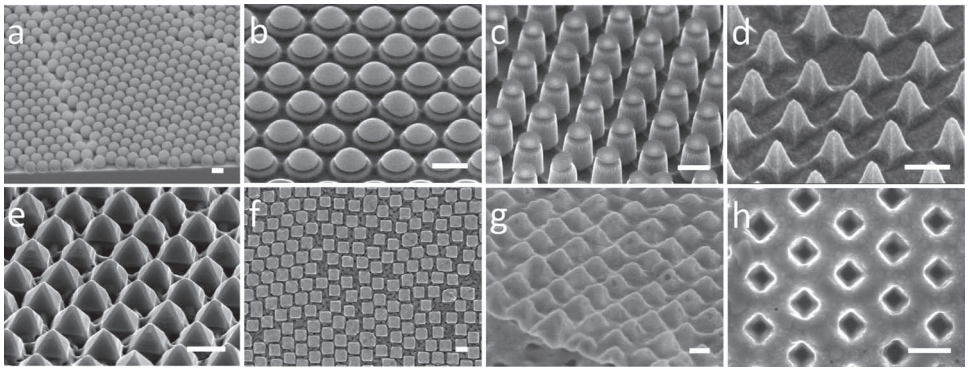

Figure 2. Scanning electron microscope (SEM) images of fabrication steps of GaAs nanopyramid thin films. All scale bars are 500 nm. a) 650 nm-diameter silica nanospheres assembled into a close packed monolayer on an epi-Ge substrate. b) Shrunk nanospheres. c) Ge nanopillars. d) Ge nanopyramids. e) 45° view of GaAs-Ge core-shell nanopyramids. f) Top view of GaAs-Ge core-shell nanopyramids. g) Front side morphology of a freestanding GaAs nanopyramids film. h) Backside morphology of GaAs nanopyramid film on PDMS superstrate.

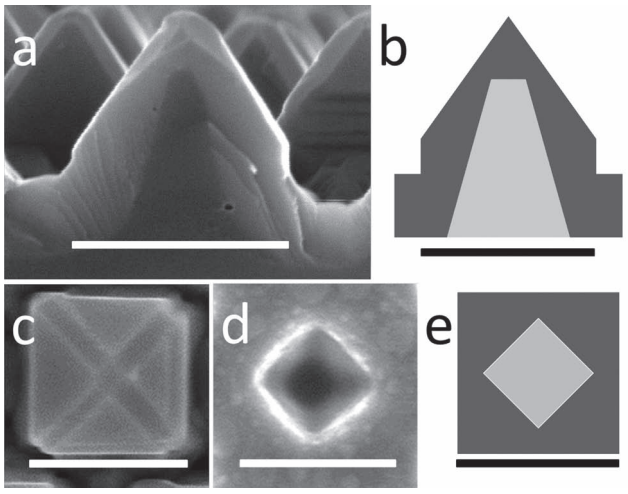

Figure 3. The zoomed-in structures of a single GaAs nanopyramid. All scale bars are 500 nm. a) SEM cross-section image of a GaAs/Ge core-shell nanopyramid. b) schematic structure of the side cross section image of a GaAs/Ge core-shell nanopyramid for simulation. c) top view SEM image of a GaAs/Ge core-shell nanopyramid. d) SEM image of backside of GaAs nanopyramid after substrate removal. e) schematic top view of a single nanopyramid structure. The inner pyramid is hollow, with a 90° rotation offset to the outer pyramid.

in Figure 3a. A top view of a nanopyramid array is shown in Figure 2f. These GaAs/Ge core-shell nanopyramid arrays can potentially enable the integration of III–V solar cells, LEDs, lasers and other optoelectronic devices on silicon substrates.

To fabricate the freestanding GaAs thin film of nanopyramid arrays, we remove the Ge/Si substrate with a gas-phase etching process. Traditional epitaxial lift-off approaches require a sacrificial AlAs layer which can be selectively removed through immersion in hydrofluoric (HF) acid.[3–5] However, HF attacks AlGaAs layers with high aluminum content. A recently proposed III–V epitaxial lift-off method uses epitaxial Ge as a sacrificial layer and XeF_2 gas for selective etching.[20] This method eliminates the need for immersion in HF solution, provides faster etching rate and preserves high aluminum content AlGaAs. In our GaAs thin film fabrication, the substrate was removed using the same gas phase etching in this lift-off process as illustrated in Figure 1f. The GaAs on Ge/Si substrate was first flipped with the GaAs nanopyramids side bonded to a Polydimethylsiloxane(PDMS) superstrate, a transparent flexible polymer film,[11] by Van der Waals force. The Ge/Si was then etched away by XeF_2 gas, leaving GaAs nanopyramid thin film on the PDMS superstrate. Figure 2g and h show the front side and the back side of a free-standing GaAs nanopyramid film, respectively. To make a comparison, a GaAs planar control film was grown on a planar Ge/Si substrate in the same MOCVD run followed by the same transfer process.

A cross-sectional SEM view of a single GaAs nanopyramid is shown in Figure 3a. The cross-sectional structure is a double-sided nanostructure after the Ge core is removed, as schematically illustrated in Figure 3b. This double-sided nanostructure is new in light trapping which will be discussed in the next section. By comparing SEM images of the front side (Figure 3c) and the backside (Figure 3d) of a single GaAs nanopyramid, one observes a 45° rotation offset between the inner and outer nanopyramids (Figure 3e). This offset is likely due to the difference in preferred facet orientations during Ge wet etching and during GaAs MOCVD growth. According to the measured dimensions in Figure 3, the average thickness of the nanopyramid film is calculated as the total volume of a nanopyramid divided by its footprint area. The nanostructured film and the planar film are both 160 nm thick. Structures in Figure 3b and 3e are also used for optical absorption simulation of the GaAs nanopyramid film in the next section.

2.2. Optical Absorption Measurements

The photograph in **Figure 4**a shows a 160 nm thick GaAs nanopyramid thin film embedded in a PDMS transparent film. The thin film can be bent to a curvature larger than 1 cm^{-1} without cracking. Absorption measurements on a GaAs nanopyramid film and its planar counterpart were taken using a standard integrating sphere system. As shown in Figure 4b, under normal

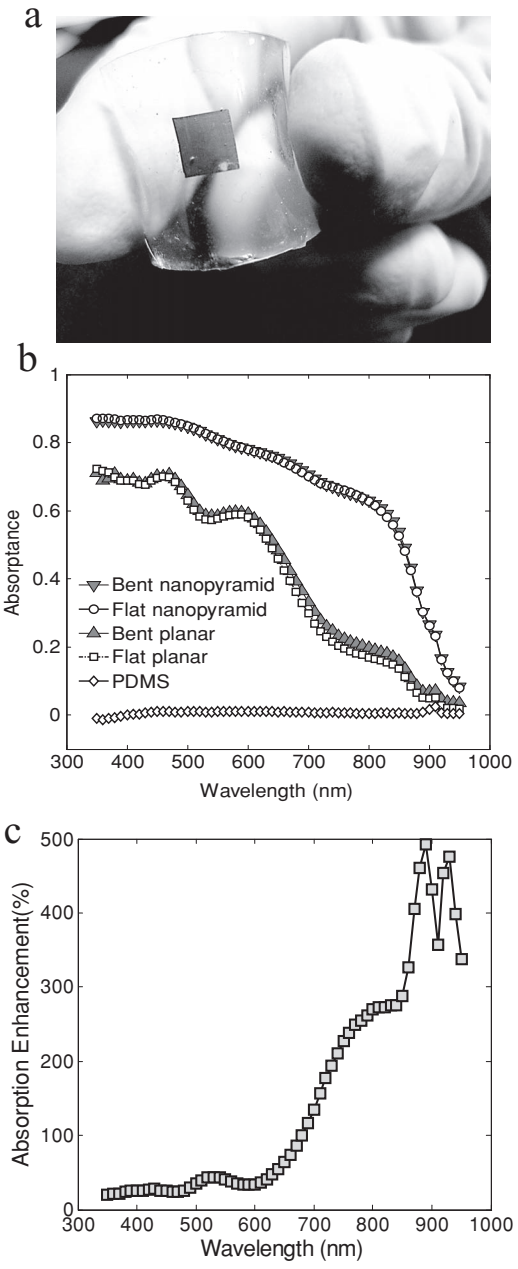

Figure 4. a) Photograph of a hand-bent GaAs nanopyramid film embedded in PDMS. b) Measured absorption spectra on samples of GaAs nanopyramid film embedded in PDMS and GaAs planar control film in PDMS at 1 cm^{-1} curvature versus at no bending. PDMS film itself is highly transparent. c) Absorption Enhancement: percentage improvement of absorption from the GaAs planar film to the nanopyramid film.

incidence, the GaAs nanopyramid sample exhibits a higher absorption than its planar counterpart over a broad spectrum of 400 nm to 1100 nm. At the short wavelengths from 400 nm to 600 nm, the enhancement (Figure 4c) is about 30%, which is largely due to the antireflection effect caused by the gradient change of refractive index from air to the GaAs nanopyramids. The enhancement increases dramatically at longer wavelengths from 700 nm to 870 nm, reaching over 300%. At long wavelengths, the absorption length is significantly increased due to the light guiding effect that couples the free space mode in air to a waveguide mode in the nanopyramid film. The absorption is not affected by a film curvature of approximately 1 cm^{-1} (Figure 4b). The flexibility and light weight in such GaAs nanopyramid films enable easy transportation and installations that could further reduce the final solar system installed cost.

To ensure that all the absorption is in GaAs, the absorption spectrum of a PDMS superstrate was also measured (Figure 4b). The PDMS superstrate has almost zero absorption over the whole spectrum despite small peaks of ~3% at 910 nm; therefore, it does not contribute to the absorption of the GaAs thin films except small peaks at 910 nm and 1020 nm. Fabry-Perot oscillations in absorption are observed on the planar control sample while the nanopyramid film shows flat broad-band absorption. These oscillations arise from the interference from the reflected and transmitted light at the two parallel interfaces between GaAs film and air. The red shift of peak positions with increasing incident angle are not significant because the optical modes inside the thin film for different incident angles are similar due to the large refractive index contrast.

Without a tracking system, solar cell performance at off-normal incident angles can significantly reduces overall electricity production throughout a day. Therefore, it is critical to maintain high absorption at large incident angles. **Figure 5**a and b show the absorption spectra at incident angles from 10° to 80° off normal incidence for the nanopyramid film and its planar control, respectively. At all incident angles and all wavelengths, the nanostructured GaAs film exhibits significant improvement in absorption over the planar film. To further investigate the absorption loss at large incident angles, absorptance versus incident angle curves at wavelengths of 400 nm, 550 nm and 700 nm are plotted in Figure 5c,d,e. Both the GaAs nanopyramid film and planar film degrade in absorption at large incident angles. However, the enhancement ratio of absorption in the nanopyramid film to the planar control increases at off-normal incident angles and reaches maximum at around 50°. In Figures 5c–e absorption curves of nanopyramid drop less in percentage from 10° to higher angles compared to their planar counterpart. Thus, nanopyramid film is less sensitive to large incident angles. With the wider angle acceptance, additional electricity could be produced over a whole day by a nanopyramid thin film solar cell in a system without sun tracking.

Total number of absorbed photons for both nanopyramid and planar films was calculated by multiplying the air mass 1.5 direct (AM1.5D) standard spectrum with the experimental data of absorption from 350 nm to 1100 nm at different incident angles. The percentage improvement in total numbers of photons absorbed by the nanopyramid film compared to the planar film at various incident angles are shown in Figure 5f. At 10° off normal incidence, the overall number of photons absorbed by the nanostructured film is 83% more than the planar control. At about 40°, the enhancement is more than 100%. Therefore, if fabricating the 160 nm nanopyramid film into a solar cell, the photocurrent can be expected to be increased accordingly by approximately 100% compared to its planar counterpart assuming the same internal quantum efficiency.

For a numerical comparison, the absorption enhancement has been calculated using a rigorous coupled-wave analysis

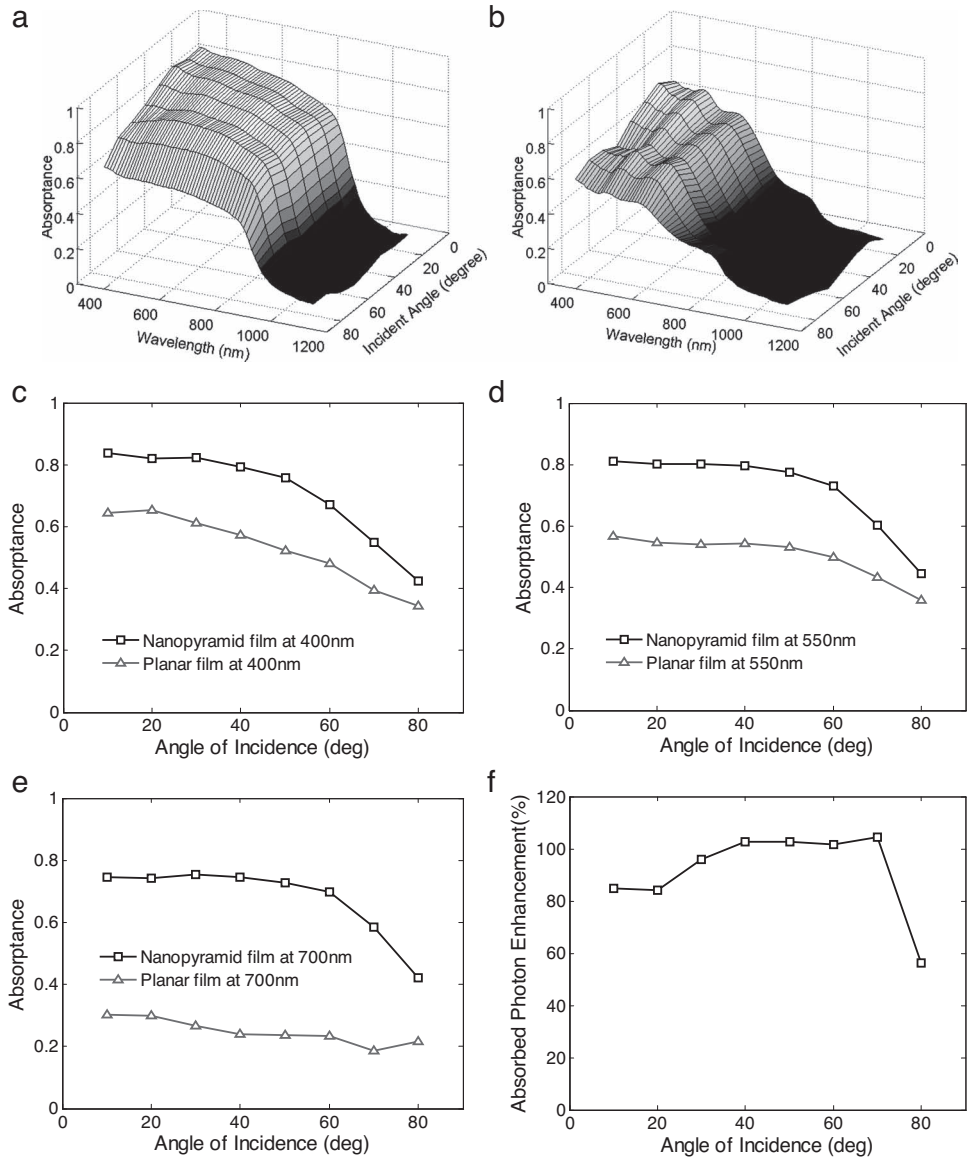

Figure 5. a) Measured absorption on GaAs planar control film on PDMS at various incident angles and wavelengths. b) Measured absorption on a GaAs nanopyramid film on PDMS transparent superstrate at various incident angles and wavelengths. c,d,e) Measured absorption on sample of GaAs nanopyramid film and its planar control at different angles of incidence at 400 nm, 550 nm, 700 nm, respectively. f) Percentage increase of total number of photons absorbed by nanopyramid film compared to that by planar films at various incident angles.

(RCWA) method.[21–23] This method provides an exact three-dimensional solution of Maxwell's equations for the experimental device geometry. The results have been averaged over both s and p polarizations for incident plane waves. The dimensions of the simulated nanopyramid are shown in Figure 3b and e, the side view and top view, respectively. The period of the nanopyramid arrays is 700 nm. The dielectric constants of GaAs are taken from tabulated experimental data,[24] and modified under the assumption that the active material is doped with germanium.[25] **Figures 6**a,b show experimental and simulation values of absorption on 160 nm thick GaAs nanopyramid film and on 160 nm GaAs planar film at incident angles of 10°, 40° and 80°. The calculated values match well with the experimental data. For the planar structure, the absorption decreases quickly as the incident angle is increased. However, in the nanopyramid structure, from normal incidence to 60° incidence, the total absorption over the entire spectrum decreases by only 5%. Compared to experimental curves for the planar film, the simulation shows more prominent oscillatory features that come from interferences at GaAs/PDMS and GaAs/Air interfaces. These features are somewhat averaged out in the experiment due to variance in actual thickness.

The physical mechanisms of absorption enhancement include anti-reflection and light trapping. On one hand, the

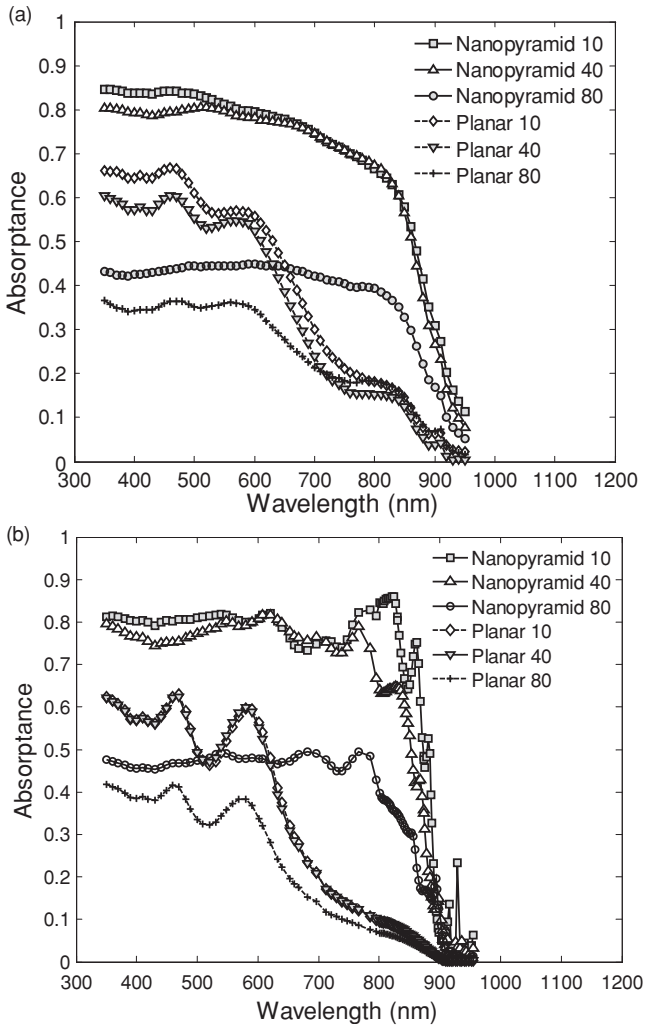

Figure 6. Experimental and simulated absorption on GaAs nanopyramid and planar films at various incidence angles. a) Experimental measurement of absorption on 160 nm thick GaAs nanopyramid film and on 160 nm GaAs planar film at incident angles of 10°, 40° and 80°. b) Calculated value of absorption on 160 nm thick GaAs nanopyramid film and on 160 nm GaAs planar film at incident angles of 10°, 40° and 80°.

nanopyramid structure essentially provides a gradual change of refractive index that greatly reduces the reflection. Simulation shows that the absorption of the nanopyramid structure is equivalent to a planar structure of 1 μm thickness, that is, approximately 57% of total number of incident photons, of which 33% of the loss is due to reflection of the incident wave, and the other 10% to imperfect absorption. On the other hand, the nanopyramid structure enhances the absorption at long wavelengths. Numerical calculations show that even assuming perfect antireflection for the planar film, a thickness of 400 nm is still needed to match the absorption of the 160 nm nanopyramid counterpart. Therefore, the improvement is not only from the antireflection effect of the front side, but also from the help of the backside nanostructures. The backside nanostructures are conformal with the front side nanopyramids, forming double-sided, waveguide-like nanostructures. These double-sided nanostructures couple the light efficiently into horizontally propagated modes, thus increase the effective optical path length of long wavelength light to multiple times of the actual film thickness.

3. Conclusion

In summary, GaAs thin film nanopyramid arrays on flexible transparent superstrates are demonstrated for the first time to the authors' knowledge. These nanostructures demonstrate excellent optical absorption properties. Without antireflection coatings, the 160 nm GaAs nanopyramid film absorbs significantly more light than its planar control film with equal thickness over a broad range of wavelengths, at various incident angles and at large bent curvatures. The 160 nm nanopyramid film is optically equivalent to 1 μm planar film without antireflection coatings or 400 nm planar film assuming perfect antireflections. The front side of these nanopyramids suppresses reflection through a gradual change of the effective refractive index while the backside nanostructures enhance absorption by forming waveguide confinement together with the front side to guide and trap long wavelength light. By combining the benefits of high absorption, high flexibility, low weight and low material cost, the nanopyramid thin film may lead to the next generation of high-efficiency and low-cost III–V photovoltaic systems.

4. Experimental Section

GaAs nanopyramid thin film transfer: A 0.5 cm^2 sample of nanopyramid GaAs on Ge/Si substrate was first flipped with the GaAs nanopyramids side attached to a PDMS film by Van der Waals force. The substrate was etched with XeF_2 gas in a Xactix etcher. After being periodically exposed to 3.0 Torr XeF_2 gas for 30 sec each cycle and 120 cycles in total, the Ge/Si was completely etched away, leaving the nanopyramid GaAs thin film attached firmly on the PDMS superstrate.

Absorption measurements: Absorption measurements of the two samples were taken using a standard integrating sphere system. A tungsten lamp coupled with a monochromator was used as the light source with a wavelength range of 300 nm to over 1100 nm. Incident light enters the sphere through a small port and illuminates the sample mounted in the center of the sphere. In order to keep all the reflected light inside the sphere, the sample was tilted by a small angle (<5°) for the normal incidence measurement. The reflected and transmitted light was scattered uniformly by the interior sphere wall. A silicon detector mounted at the back of the sphere produces a photocurrent of all the non-absorbed photons. Before measuring the samples, a photocurrent spectrum was taken for the empty sphere, serving as a reference. Another photocurrent spectrum was then taken after mounting the sample in the sphere. The ratio of these two photocurrent responses gives the total amount of reflectance $R(\lambda)$ and transmittance $T(\lambda)$ of the thin film. Absorptance $A(\lambda)$ can then be obtained by $A(\lambda) = 1 - R(\lambda) - T(\lambda)$. In order to eliminate systematic errors due to the possible intensity drift of the light source, a reference diode was used to monitor and compensate for such changes. Errors were controlled and reassured to be within 1%. For measurement on bent films, curvatures were created by mounting the films onto a transparent 10 mm diameter tube. For incident angle dependence measurements, the sample was rotated from 10° to 80° with 10-degree steps.

Received: January 7, 2012
Published online: May 31, 2012

[1] D. Ginley, M. A. Green, R. Collins, *MRS Bull.* **2008**, *33*, 355.
[2] M. A. Green, K. Emery, Y. Hishikawa, W. Warta, E. D. Dunlop, *Prog. Photovolt: Res. Appl.* **2011**, *19*, 565.
[3] E. Yablonovitch, T. Gmltter, J. P. Harbison, R. Bhat, *Appl. Phys. Lett.* **1987**, *51*, 2222.
[4] J. Yoon, S. Jo, I. S. Chun, I. Jung, H. Kim, M. Meit, E. Menard, X. Li, J. J. Coleman, U. Paik, J. A. Rogers, *Nature* **2010**, *465*, 329.
[5] J. J. Schermer, G. J. Bauhuis, P. Mulder, E. J. Haverkamp, J. van Deelen, A. T. J. van Niftrik, P. K. Larsen, *Thin Solid Films* **2006**, *511*, 645.
[6] O. D. Miller, E. Yablonovitch, S. R. Kurtz, *arXiv* **2011**, 1106.1603, 1.
[7] M. Putnam, S. Boettcher, M. Kelzenberg, D. Turner-Evans, J. Spurgeon, E. Warren, R. Briggs, N. Lewis, H. Atwater, *Energy Environ. Sci.* **2010**, *3*, 1037.
[8] E. Garnett, P. Yang, *Nano Lett.* **2010**, *10*, 1082.
[9] T. Hsueh, C. Hsu, S. Chang, P. Guo, J. Hsieh, I. Chen, *Scr. Mater.* **2007**, *57*, 53–56.
[10] Y. Dong, B. Tian, T. Kempa, C. Lieber, *Nano Lett.* **2009**, *9*, 2183.
[11] Z. Fan, H. Razavi, J. Do, A. Moriwaki, O. Ergen, Y. Chueh, P. Leu, J. Ho, T. Takahashi, L. Reichertz, S. Neale, K. Yu, M. Wu, J. Ager, A. Javey, *Nat. Mater.* **2009**, *8*, 648.
[12] J. Zhu, Z. Yu, G. F. Burkhard, C. Hsu, S. T. Connor, Y. Xu, Q. Wang, M. McGehee, S. Fan, Y. Cui, *Nano Lett.* **2009**, *9*, 279.
[13] J. Zhu, C. Hsu, Z. Yu, Z. Fan, Y. Cui, *Nano Lett.* **2010**, *10*, 1979.
[14] B. M. Kayes, H. A. Atwater, N. S. Lewis, *J. Appl. Phys.* **2005**, *97*, 114302.
[15] G. Mariani, P.-S. Wong, A. M. Katzenmeyer, F. Leonard, J. Shapiro, D. L. Huaker, *Nano Lett.* **2011**, *11*, 2490.
[16] P. J. Poole, D. Dalacu, J. Lefebvre, R. L. Williams, *Nanotechnology* **2010**, *21*, 295302.
[17] J. A. Czaban, D. A. Thompson, R. R. LaPierre, *Nano Lett.* **2009**, *9*, 148.
[18] D. Choi, Y. Ge, J. S. Harris, J. Cagnon, S. Stemmer, *J. Cryst. Growth* **2008**, *310*, 4273.
[19] K. Mizuguchi, N. Hayafuji, S. Ochi, T. Murotani, K. Fujikawa, *J. Cryst. Growth* **1986**, *77*, 509.
[20] G. D. Cole, Y. Bai, M. Aspelmeyer, E. A. Fitzgerald, *Appl. Phys. Lett.* **2010**, *96*, 261102.
[21] S. G. Tikhodeev, A. L. Yablonskii, E. A. Muljarov, N. A. Gippius, T. Ishihara, *Phys. ReV. B* **2002**, *66*, 045102.
[22] L. Li, *J. Opt. Soc. Am. A* **1997**, *14*, 2758.
[23] V. Liu, S. Fan, S4: A free electromagnetic solver for layer periodic structures, http://www.stanford.edu/group/fan/S4. Accessed date: January, **2012**.
[24] E. D. Palik, *Handbook of Optical Constants of Solids II*, Academic Press, NY, USA **1991**.
[25] H. C. Casey Jr., D. D. Sell, K. W. Wecht, *J. Appl. Phys.* **1975**, *46*, 250.